Automatic Detection of Defects in Tire Radiographic Images

Yan Zhang, Dimitri Lefebvre, and Qingling Li

***Abstract*—This paper is about the detection of tire defects in multi-textural radiographic images. We consider the tire defects characterization problem in ways of local regularity analysis and scale characteristic. Optimal scale and threshold parameters are selected using a defect edge measurement model to frame defect edge detection. This framework distinguishes the defects from the background textures. Finally, a novel method for detection of tire defects is proposed based on wavelet multiscale analysis. We provide examples with a consistent dataset of 400 images selected over 3700 industrial images in order to illustrate and validate the obtained results which demonstrate substantial improvement over the state of the art.**

Note to Practitioners—**Defects detection is a major challenge in numerous industrial applications. This contribution is of particular interest for tire manufacturers for which pneumatic tire defect detection mainly rely on human vision. Using computer-based technologies and signal processing methods based on wavelet transform, this paper proposes an efficient approach to implement the detection operations in a systematic way. Moreover, the proposed method is also extendable to other defect detection problems with image processing.**

***Index Terms*—Defect detection, pneumatic tire, radiographic image, wavelet multiscale analysis.**

I. Introduction

NONDESTRUCTIVE testing (NDT) techniques have been employed to test a material for surface or internal flaws without interfering in any way with its suitability for service [1]. The most commonly used methods include acoustic emission, magnetic particle inspection, eddy current, ultrasonic testing, thermal inspection, and several others. Such methodologies have been widely applied in various application domains such as steel [2], castings [3], [4], textile [5], TFT-LCD panel [6], nanostructures [7], [8], titanium-coated aluminum surfaces [9], and semiconductors [10]. Computer vision-based methodologies can be categorized as laser shearography image-based methods [1], X-ray radiography images-based methods [11], and CCD camera optic images-based methods [12]. Laser shearography has been widely used as an important technology in surface defect detection [13] in rubber and tire industries. Radioscopy (X-ray or gamma ray), on the other hand, is another effective tool which has been widely used in industrial applications such as weld defect detection and casting defect detection [14]–[16]. Much work has been also done on automatic surface defect detection using CCD camera optic images [17] and scanning electron microscope [18].

Although in the tire industry X-ray inspection systems have been applied to carry out computer vision, automatic defect inspection and identification is still done by a human observer in many tire manufacturing companies. Such a detection process is time consuming, inefficient, subjective, and even biased under high working intensity. There are certain major difficulties in systematic pneumatic tire defect detection due to the characteristics of pneumatic tire radiography images, given here.

1) The image intensity varies significantly because tires are complex laminated composite structures. Different types of tires or different parts of the same tire differ in structure, thickness, and rubber materials which also contribute to unevenness of intensity. The intensity of defects regions is often similar to the cord texture in tires.
2) There are different kinds of defects of different forms, shapes, intensities, and scales such as bubble defects, foreign object defects, various cord defects, and crack defects. The feature space for these defects is not compact.
3) Texture patterns of different parts of a tire vary such that inhomogeneous background is a significant challenge for automatic defect detection.

Compared with other computer vision applications, research on pneumatic tire defect detection is still quite limited. In the literature, inspection methods based on statistical, spectral, model-based, learning, structural, and motif-based approaches were proposed.

The speckle-based methods, together with the edge features, have been used in tire defect detection for more than thirty years [19]. In [1], a tire defect detection method using laser shearography was proposed combining curvelet-based image enhancement and Canny operator to detect defects in laser shearography image. Based on the characteristic that edge features correspond to larger curvelet coefficients in subhighest frequency band, curvelet coefficients were modified to enhance image edges before further edge detection operations. The method reached satisfactory performance toward tire bubble

Manuscript received January 22, 2015; revised May 21, 2015; accepted August 13, 2015. This paper was recommended for publication by Associate Editor C. Mahulea and Editor M. P. Fanti upon evaluation of the reviewers' comments. This work was supported in part by the Shandong Provincial Natural Science Foundation under Grant ZR2014FL021 and by the China Scholarship Council Foundation under Grant 201207890008.

Y. Zhang is with the College of Electromechanical Engineering, Qingdao University of Science and Technology, Qingdao 266061, China (e-mail: zy@qust.edu.cn).

D. Lefebvre is with the Normandie Université, Le Havre 76600, France (e-mail: dimitri.lefebvre@univ-lehavre.fr).

Q. Li is with the College of Electromechanical Engineering, Qingdao University of Science and Technology, Qingdao 266061, China (e-mail: liqingling@qust.edu.cn).

Color versions of one or more of the figures in this paper are available online at http://ieeexplore.ieee.org.

Digital Object Identifier 10.1109/TASE.2015.2469594

defect and carcass delamination defect detection. However, there are critical limitations for laser shearography-based nondestructive testing methods; for example, vacuum status is necessary to obtain the interfere image, and the detection performance for nonmetallic foreign objects like plastic is limited. Xiong *et al.* [20] combined digital image correlation and phase shifting method to detect tire defects. A quantitative detection of internal defects in tires by an interferographic technique is suggested by Chien *et al.* in [21].

In our previous research, we have indicated a foreign bodies defects and bubble defects detection in tire X-ray radiography images based on total variation image decomposition and edge detection [11]. Tire radiography images were first decomposed into texture parts and cartoon parts using total variation. In the cartoon component, the intensity of foreign bodies and bubble defect regions distinguishes from the background and defects were detected using edge detection techniques. The scheme works successfully for detecting defects. However, the contours of detected defects are inaccurate and incomplete such that it is difficult to extract complete defect information. In [22], Ng *et al.* also applied image decomposition to inspect and visualize defective objects in a patterned fabric image. Their detection accuracies ranged from 94.9%–99.6% according to different types of defects. Li [23] probed into radial tire defect detection in X-ray radiography images based on fuzzy edge detection method. Gayer and Saya [24] proposed a scheme for detecting defects during the manufacture of steel-belt tires. In [25], a dictionary representation-based tire defect detection algorithm was proposed. The distribution difference of representation coefficients was used as a discrimination criterion to detect the defective region. Experimental results were compared with that of automatic band selection for wavelet reconstruction method introduced in [26] which indicated that it was difficult to detect defects with illumination variation. Zhu proposed a bubble defect detection method in tires using digital holography [27]. Methods based on a ground truth or templates evaluate the difference between the image and the template to detect defects [28].

Unfortunately, numerous research works for tire defect detection are not reported in the literature due to the constraints in intellectual property right because most of the techniques are used in commercially systems. In automatic defect inspection applications, such as defect detection for fabric, steel, casting and weld etc., the objectives of them are, similar to tire defect detection, to detect, identify, and locate defects of patterned or unpatterned, grayscale or color, structures during manufacturing. In [29], a regularity analysis method was described for patterned texture inspection. Motif-based patterned texture defect detection methods including Fourier transform [30], wavelet transform [31], Gabor transform [32], pattern matching [33], co-occurrence matrices [34]-based methods were evaluated for 2-D patterned texture images in [35]. Among them, wavelet-based methods have received great attention. Ghorai *et al.* proposed an automatic defect detection method for flat steel using wavelet features derived from contiguous pixel blocks [36]. A wavelet-based subimage binarization method developed by Li [15] could effectively be used to detect casting defects which are distinguished by local changes in the image intensity. Li and Tsai [37] used wavelet coefficients in individual decomposition levels as features and the difference of the coefficient values between two consecutive resolution levels as the weights to distinguish local defects to detect defect in solar wafer. Ngan *et al.* proposed a wavelet subimages preprocessed golden image subtraction method for defect detection on patterned fabric or repetitive patterned texture [38]. Mak *et al.* proposed a fabrics automated inspection scheme for fabrics defects based on Gabor wavelet network and morphological filters [39]. A Gabor wavelet network was used to extract basic texture features as the *priori* knowledge for detection in the method whose detection accuracy reached 97.4% on their dataset. All of these methods mentioned above extract wavelet coefficients of smooth or detail subimages at certain decomposition levels as local features and classify defects from them. However, these methods including adaptive intensity thresholding and template-based methods would not be suitable for tire defect detection because of the characteristics of tire radiography images discussed above. Previous approaches may be effective in detecting certain types of defects under certain conditions, but they are restrictive and insufficient for automatic tire defect detection applications.

To reach an accurate and complete defect detection, in this paper, a wavelet multiscale representation methodology for pneumatic tire defect detection in radiography images is proposed. Unlike the conventional wavelet-based defect detection methods which focus on extracting the discriminated subimage features in wavelet domain, in this work, the properties of multiscale edges in pneumatic tire radiography image are discussed through wavelet analysis. We address the problem of tire defects characterization by local regularity analysis of signals. The influence of wavelet scales and wavelet maxima values on three different edge models are introduced and discussed based on which edges generated from different types of objects can be separated. Optimal scale and threshold parameters are selected using a defect edge measurement model to frame defect edge detection. The optimal parameters framework distinguishes the scale characteristics between defects and background textures. Finally, a template generation method is indicated to localize defects using the proposed minimum occlusive edge linking and mathematical morphology methods.

This paper is organized as follows. We present theoretical foundations of the wavelet modulus maxima edge and the influence of parameters on different edge models in Section II. In Section III, we propose and study an automatic defect detection method based on wavelet edges for tire radiography image. Experimental results and discussions are introduced in Section IV, including a comparison results of regular methods. Finally, conclusions are delivered in Section V.

II. System and Techniques

A. Wavelet Analysis and Modulus Maxima Edge

Wavelet analysis has attracted much attention recently in signal processing and has been successfully applied in many applications such as transient signal analysis, image analysis, fault detection and diagnosis, and communications systems.

Localizations in time and frequency domains can be achieved using wavelet analysis which provides a multiresolution approach to image analysis. The advantage has attracted tremendous focus especially in signal and image processing.

Edges are critical to discriminate objects from their background and therefore play very important roles in a variety of applications such as object detection, region segmentation, image retrieval, data hiding or recognition and tracking of objects in image sequences. Wavelet transform has been used for edge detection in previous works by researchers such as Mallat and Zhong [40], Merlet and Zerubia [41], Hsieh *et al.* [42], and Aydin *et al.* [43]. In [44], Waghule and Ochawar reviewed wide range of methods of edge detection and concluded that wavelets based methods are more accurate than other methods (i.e., Canny operator).

Singularities of a signal can be characterized by the modulus of their wavelet transforms [45]. A numerical technique for characterizing 2-D discrete signals in terms of multiscale edges is introduced in this section. With an appropriate choice of wavelet, the locations of edges correspond to modulus maxima of the wavelet transform at a given scale. The modulus maxima are used to calculate Lipschitz exponents of edges which describe the sharpness of an edge. Due to the fact that image edges are often non-derivable and sometimes discontinuous, a 2-D smoothening function $\theta(x, y) \in L^2(\mathrm{R})$ is defined to smooth the image. The derivatives of Gaussian functions are widely used as mother wavelets for signal and image analysis since they provide the best resolution in time and in frequency and important signal features such as extremum, inflection point, edge, local regularity, and singularity can be detected. The first-order partial derivative in horizontal and vertical directions of the derivable 2-D smoothening function are taken as mother wavelets defined as

$$\psi^1(x, y) = \frac{\partial \theta(x, y)}{\partial x}, \psi^2(x, y) = \frac{\partial \theta(x, y)}{\partial y}. \tag{1}$$

At scale $s = 2^j$, the functions in (1) are dilated as

$$\psi_j(x, y) = \left(\frac{1}{2^j}\right)^2 \psi(\frac{x}{2^j}, \frac{y}{2^j}). \tag{2}$$

The 2-D wavelet transform of image function $f(x, y)$ on scale s is defined as

$$W_j^{(1)} = \left\langle f(x, y), \psi_j^{(1)}(x, y) \right\rangle \tag{3a}$$

$$W_j^{(2)} = \left\langle f(x, y), \psi_j^{(2)}(x, y) \right\rangle. \tag{3b}$$

They are the first-order derivative of the smoothening image along horizontal and vertical direction respectively. Namely they are the two gradient vector components of the image $f(x, y)$ smoothed by function $\theta_j(x, y)$. It can be proved that

$$\begin{aligned} \begin{bmatrix} W_j^{(1)} \\ W_j^{(2)} \end{bmatrix} &= 2^j \begin{bmatrix} \frac{\partial}{\partial x} \langle f(x, y), \theta_j(x, y) \rangle \\ \frac{\partial}{\partial y} \langle f(x, y), \theta_j(x, y) \rangle \end{bmatrix} \\ &= 2^j \nabla \langle f(x, y), \theta_j(x, y) \rangle. \end{aligned} \tag{4}$$

The two components of the wavelet transform are directly proportional to $\langle f(x, y), \theta_j(x, y) \rangle$. To locate the positions of abrupt variations of $f(x, y)$, namely, the edges of the image, we should therefore consider the local maxima of the gradient magnitude at various scales. The modulus of the wavelet transform at scale 2^j is given by

$$\begin{aligned} M_j(f(x, y)) &= \| 2^j \nabla \langle f(x, y), \theta_j(x, y) \rangle \| \\ &= \sqrt{(W_j^{(1)} f(x, y))^2 + (W_j^{(2)} f(x, y))^2}. \end{aligned} \tag{5}$$

At a large scale, the small-signal fluctuations are removed by the convolution such that the sharp variations of large structures are detected and vice versa. The phase angle of gradient vector in any direction is given by

$$A_j(f(x, y)) = \arctan\left(\frac{W_j^{(2)} f(x, y)}{W_j^{(1)} f(x, y)}\right). \tag{6}$$

Wherever the modulus $M_j(f(x, y))$ of the wavelet transform attains a local maximum in the direction of the gradient $A_j(f(x, y))$, there is an edge point at point (x, y) at scale 2^j.

There are numerous wavelet functions that can be used for edge detection such as the first derivative of Gaussian function, the second derivative of Gaussian function, the nth derivatives of Center B-Spline function, and quadratic spline wavelet function. These wavelet bases are evaluated for edge detection in previous studies, and the results indicate that the effect of different wavelet bases on edge detection is limited [46]. In this study, we define $\theta(x, y)$ as the Gaussian function with dispersion parameter σ as

$$\theta(x, y) = e^{-(x^2+y^2)/2\sigma^2} \tag{7}$$

and we select the derivatives of $\theta(x, y)$ as mother wavelet functions

$$\frac{\partial \theta}{\partial x} = -\frac{x}{\sigma^2} e^{-(x^2+y^2)/2\sigma^2} \qquad \frac{\partial \theta}{\partial y} = -\frac{y}{\sigma^2} e^{-(x^2+y^2)/2\sigma^2}. \tag{8}$$

To detect edges at a given scale j, (8) are convoluted with the preprocessed image respectively. Gradient magnitude and direction of each pixel are computed using (5) and (6). Edges are detected and built according to variations of the modulus and gradient direction using a thresholding method as in

$$|M_j(f(x, y)) - M_j(f(x_0, y_0))| \leq E \tag{9}$$

$$|A_j(f(x, y)) - A_j(f(x_0, y_0))| < \delta. \tag{10}$$

If both criteria are satisfied, namely, if each pixel with coordinates (x_0, y_0) in neighborhood of (x, y) is similar in magnitude and in angle to pixel at (x, y), then edge pixel (x_0, y_0) is linked with (x, y).

B. Influence of Wavelet Parameters on Edge Model

In wavelet multiscale edge detection, weak or strong edges with different scale characteristics can be obtained by using different thresholds and scale parameters. In comparison, conventional edge detectors such as Prewitt and Sobel are poorly adjustable. However, a conventional Canny edge operator is adjustable, it does not examine edges at all scales, the result can still be affected by strong noise, and there is a lack of adaptive parameter method for automatic detection. It cannot yield a

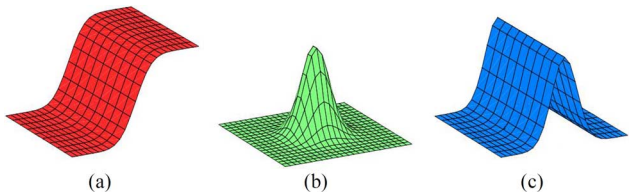

Fig. 1. Edge models. (a) Transition edge. (b) Peak edge. (c) Line edge.

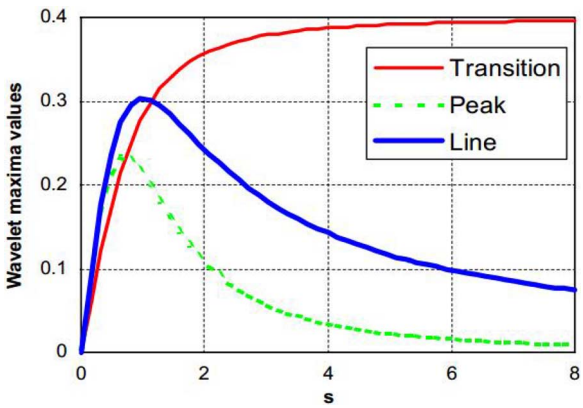

Fig. 2. Wavelet maxima values associated to the transition edge, the peak edge and the line edge versus scale s.

complete and stable representation using canny edges in two dimensions [40]. Wavelet transform brings forward a possibility of constructing a variety of edge detectors with proper scales that meet different requirements.

The key issues of wavelet multiscale edge-based defect detection would be first to make a distinction between the edges of defect and that of background texture and second to obtain the optimal parameters. To achieve this, it is important to study the influence of parameters on different edge models. There are three typical edge models in tire radiography images that correspond to cord, noise, and defect (Fig. 1).

To address the tire defect detection problem using wavelet edges, two issues are considered. Which modulus maxima at different scales correspond to the defect edges? How can one discriminates the modulus maxima that corresponds to the defect edges effectively? In [47], Ducottet *et al.* studied the influence of scales on the transition edge, the peak edge, and the line edge.

Three edge functions corresponding to the edge models are defined from a smoothing of the three types of singularities, and their wavelet transforms are determined. Then, the modulus value of the local maximum in the direction of the argument are calculated. The transition edge function is strictly increasing and has an horizontal asymptote while the scale increases, while the peak edge function and the line edge function decrease around $s = 1$ like a power -2 and a power -1 at infinity respectively (Fig. 2).

III. Tire Defect Detection Using Wavelet Edges

Defects are characterized in radiographic images by local changes in the image intensity, resulting in corresponding local discontinuities in the gray values [46]. The typical foreign object tire defects in radiographic images correspond to transition edge in wavelet multiscale edge maps while the cord texture and background correspond to the line edge and peak edge, respectively. Moreover, noise in radiographic images is characterized by its high spatial frequency and its lack of spatial correlation. It is therefore applicable to separate transition edge from the cord texture and background by choosing appropriate wavelet maxima value threshold and scale.

In this work, some preprocessing methods are used. Noise reduction is typically carried out by median and Wiener filters while keeping satisfied edge retention effect. On the other hand, in wavelet edge detection the mathematical expectation of noise signal satisfy

$$E\left(|M_j(n(x,y))|^2\right) = \frac{\sigma^2\left(\left\|\psi_j^{(1)}\right\|^2 + \left\|\psi_j^{(1)}\right\|^2\right)}{2^j} \qquad (11)$$

where $n(x,y)$ is the noise and σ^2 is the variance of $n(x,y)$. When the scale increases the mathematical expectation of noise decreases multiplicatively (Fig. 2). Peak edges corresponding to noises in an image can be diluted by wavelet multiscale edge method. Adaptive histogram equalization (AHE) is used to enhance contrast in various applications such as medical image enhancement and other initially nonvisual ones. Tire radiography images contain bright or dark regions caused by rubber thickness variation on which global histogram equalization will not work effectively. These regions result in fake line edge as well as partial missing of important edge information. AHE method is used in this work by considering only small regions to perform contrast enhancement of those regions.

Directionality and local variation of intensity are the major elements to rely upon for solving the defect detection and classification problem. A practical solution for this application should be able to estimate at the same time how and how much the intensities vary in the image, in order to select defects that produce sharp variation points (edge points) with high directionality. In general the ambiguity introduced by multiple scale is inescapable. It is important to detect a complete and accurate defect edge for further processing such that it is essential to reduce the ambiguity by deciding which scales s and thresholds T is optimal for representing wavelet transform modulus maxima defect edges.

To achieve this, we experiment on tire radiographic images using a series of scales and thresholds. If the intensity contrast is sufficiently strong with respect to the critical level T, then an edge is detected. Wavelet modular images can be obtained with different resolutions by applying a variety of scales in each of which a certain amount of edge information is provided. With higher resolution, namely at a small scales, the locating accuracy is relatively higher while weaker edges are detected. Therefore, the detection is sensitive to noise and may result in fake edges at small scales. On the contrary, with low resolution, namely at a large scale, the locating accuracy is relatively lower while only strong edges can be detected as illustrated in Fig. 3(f)–(j) with $T = 0.2$ and $j = 1, 2, 3, 4, 6$, respectively.

When $j = 2$, the defect boundary is complete and accurate, and few background texture edges and noise are detected. Also, it is worth noting that, compared with the texture edges in the background, edges of defect have larger scale, which indicates

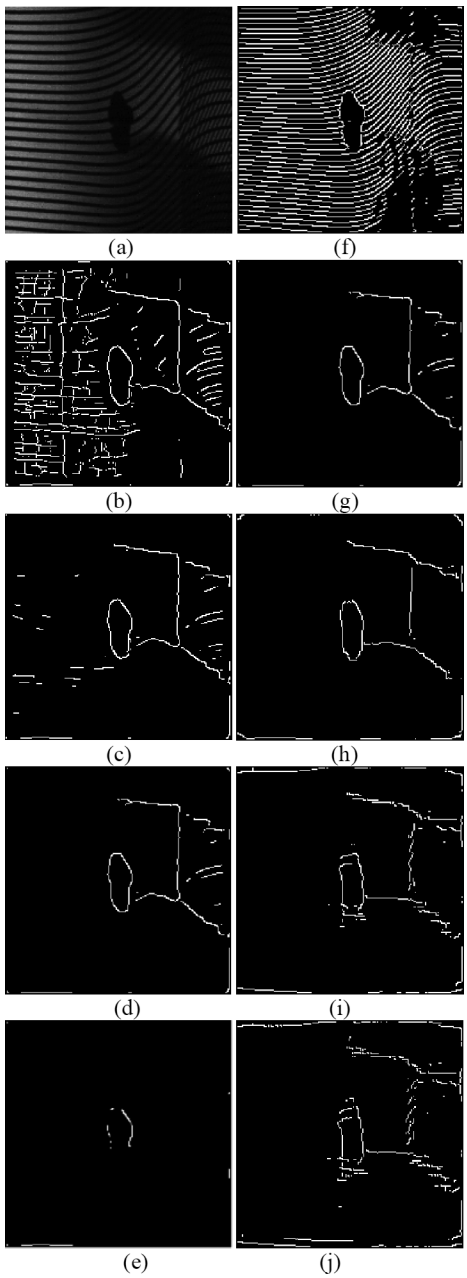

Fig. 3. (a) Wavelet transform modulus maxima edge detection experimental results. (b)–(e)$j = 2$, $Threshold = 0.05, 0.15, 0.2, 0.5$, respectively. (f)–(j) $Threshold = 0.2$, $j = 1, 2, 3, 4, 6$, respectively.

that edges of defect boundary yield larger wavelet responses than texture edges in background regions at larger scales in wavelet transform.

When $j > 3$, with the increment of scale, only subtle changes occur and the edge of defect becoming distorted. In other words the locating accuracy is becoming lower [Fig. 3(i) and (j)].

As can be seen in Fig. 3(a)–(e), a set of thresholds are tested on the given test image at scale $j = 2, T = 0.05, 0.1, 0.2, 0.5$, respectively. These results indicate that defect edges as well as weak edges and even unexpected noise which interfere defect locating are detected at a certain scale with a low threshold value. With a higher threshold, only strong edges that represent defect boundary and few incomplete background texture edges are selected. When the threshold is too high, for example $T = 0.5$ in Fig. 3(e), no background texture edge is detected, however, the defect boundary edge becomes incomplete even though it is accurate in shape and location.

From the above discussions, it can be concluded that to obtain a complete and accurate defect edge without noise and background details, optimal threshold and scale parameters selection are important tasks. How accurate the edges are and how many edges we would like to obtain can be decided by appropriate wavelet scale and threshold in the application of defect detection for reasonable and effective results. In the following, we select optimal threshold value T and scale value j using an edge detection performance measurement method.

In order to measure the accuracy of the detected defect edges we introduce the well-known figure of merit (FOM) F and the localization accuracy D given by

$$F = \frac{1}{\max(N_I, N_A)} \sum_{k=1}^{N_A} \frac{1}{1 + \alpha d^2(k)} \tag{12}$$

$$D = \sqrt{\frac{1}{N} \sum_{k=1}^{N_A} d^2(k)} \tag{13}$$

where N_I is the number of the actual edges, N_A is the number of the detected edges, N is the total number of true edges that are detected, and $d(k)$ denotes the distance from the kth actual edge to the corresponding detected edge. To be consistent with other research work [48], [49], we set the scaling constant α to 0.11. The mean square distance D from the actual edges to the detected ones gives the localization accuracy. ζ is the factor that compromises between the accuracy, defect edge pixels and background edge pixels to guarantee *EM* reaches optimal which is given as

$$\zeta = \begin{cases} 0.1, & \text{if } \sum P_d > 2^* \sum p_b \\ 1, & \text{if } \sum p_b < \sum p_d \le 2^* \sum p_b \\ 20, & \text{if } \sum p_d \le \sum p_b \end{cases} \tag{14}$$

where $\sum p_d$ and $\sum p_b$ are the number of pixels in defect edges and background edges. Finally the edge detection performance measurement model *EM* is given to evaluate both the defect edge localization accuracy and shape accuracy:

$$EM = \frac{F}{\zeta D}. \tag{15}$$

To compute *EM*, first, the ground truth defect edges are extracted for defective tire radiography images in the test dataset. Secondly, the data set is tested using wavelet modulus maxima edge detection at different scales with different thresholds. Finally, the FOM function F and the localization accuracy function D are computed and the *EM* values for different parameters are measured using (15). The *EM* values are normalized and plotted in Fig. 4 with respect to parameters j and T. The scale $j = 2$ with threshold $T = 0.23$ leads to the maximal value of indicator *EM*. These values of the parameters characterize at best the defect edges.

However, defect edges can be detected small pieces of defect edges may be missing while strong large-scale background transition edge may be residual. These can be caused by structure,

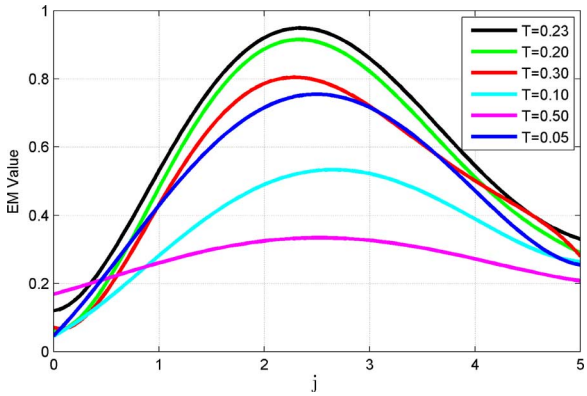

Fig. 4. Normalized edge detection performance scores.

thickness, and rubber materials of the tire tested which result in the unevenness of intensity in an radiographic image.

To remove the residual background noise, weak edges and thereafter to generate defect template, a minimum occlusive edge linking and mathematical morphology operations are applied. Interconnected edges larger than 20 pixels (the value depends on the resolution of tire inspection vision system and enterprise's defect standard, in tire production industries a foreign objects smaller than 2 mm are considered indefective.) are selected and labeled as $e_i, i = 0, 1, 2 \ldots n$ if the edges are not occlusive. The endpoints set of selected edges are defined as

$$\left\{e_i \left[p_i^h(x,y), p_i^t(x,y)\right], i = 0, 1, \ldots n\right\} \tag{16}$$

where $p_i^h(x,y)$ and $p_i^t(x,y)$ are the head point and tail point of edge e_i, respectively. We search for a minimum occlusive edge using a decreasing threshold in a more detailed edge map for all or a part of the endpoints under the constraint that the connection length is minimum.

Then, the minimum occlusive edge is filled and proceeded by performing mathematical morphology operations to eliminate burrs. A square 3×3 structuring element S is used for the basic operations of erosion and dilation. The erosion $A\Theta S$ is defined to be the set of all pixel locations for which S placed at that pixel is contained within A as

$$A\Theta S = \{(x,y) : S(x,y) \subset A\} \tag{17}$$

where A is a set (a binary image or a part of it). If A^c denotes the complement of A, then the dilation of a set A by a set S is defined by $A \oplus S$ as

$$A \oplus S = (A^c \Theta S)^c. \tag{18}$$

After these post-processing operations, a clear defect edge map without nondefective edges and noise can be obtained. Finally, defects are segmented from the test images using the defect maps and defect shape features, for example, intensity, diameter, area, length, and width, are extracted to provide features for further offline defect classification processing.

IV. Experimental Results and Discussions

Here, experiments on pneumatic tire radiography images were performed. Test images were obtained from pneumatic radial light truck and car tires using X-ray inspection vision systems. The dataset for the experiments contains 3700 tire radiographic images with 256 gray levels from 30 types of tires with different surface textures and cord patterns. Among them, 3500 images are defect-free tire images, 200 images are defective tire images.

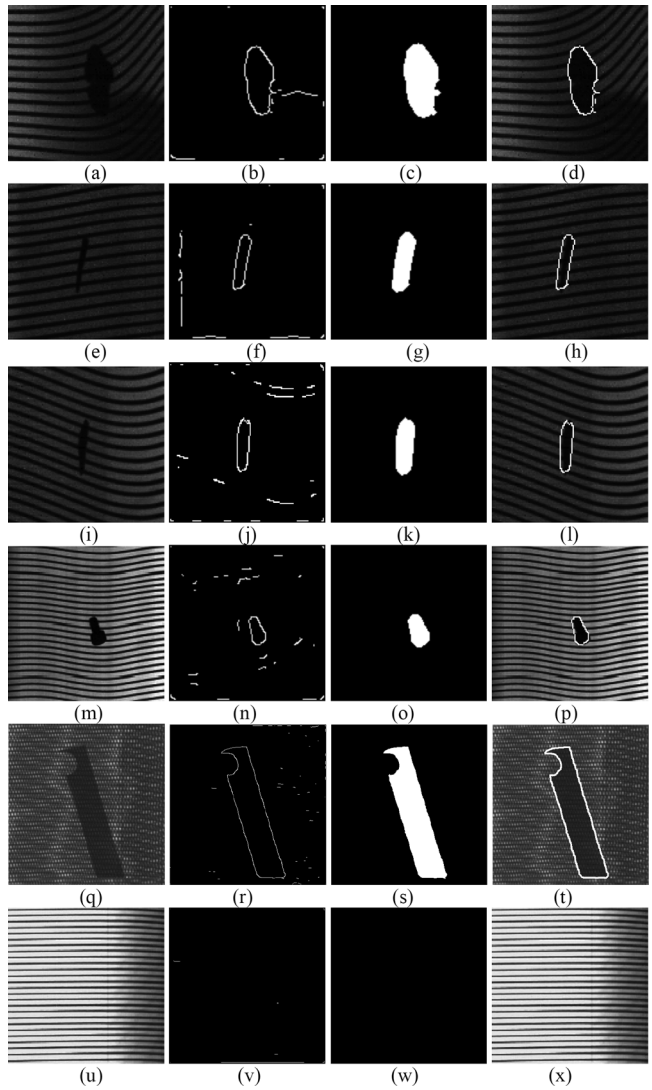

Fig. 5. Experimental results on both defect and defect-free test images with different intensities, scales and defect patterns: (a), (e), (i), (m), (q), and (u) are test image; (b), (f), (j), (n), (r), and (v) are defect edges detected before morphology operation; (c), (g), (k), (o), (s), and (w) are defect segmentation mask generated; (d), (h), (l), (p), (t), and (x) are final defect detection and segmentation results.

Experiments were performed on a selected dataset in which there are 400 images (200 defective tire images and 200 selected typical defect-free tire images) which vary in unevenness of intensity, scale as well as background texture patterns to validate the robustness of the scheme. Two hundred images (100 defective and 100 defect-free) were used for the optimal parameters selection of the algorithm, and another 200 images were used as test images.

Conventional edge detection methods (such as Canny, LoG, Sobel, and Level set), scale space blob detection and scale-invariant feature transform (SIFT) key points detection methods

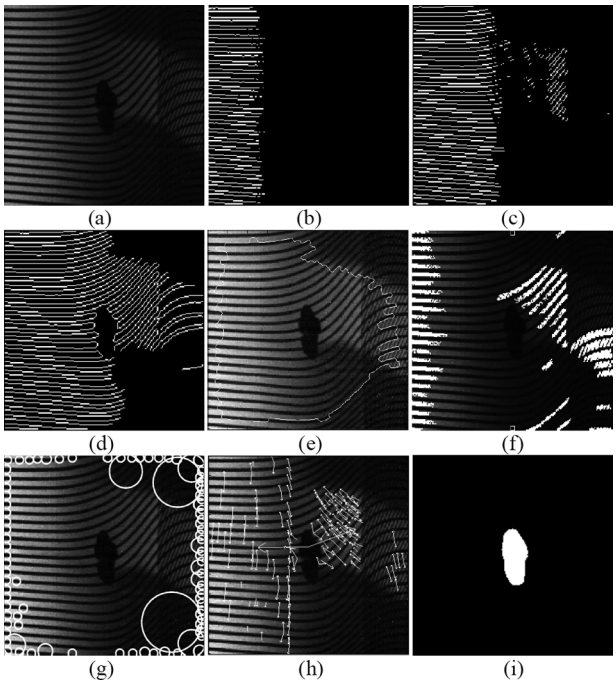

Fig. 6. Edge detection experimental results comparison. (a) Test image. (b) Sobel method. (c) LoG method. (d) Canny method. (e) Level set method. (f) Watershed method. (g) Scale space Blob method. (h) SIFT features. (i) Proposed scheme.

are applied to the test data set for comparison issue. We apply the scheme on defect and defect-free images with different intensities.

Experiments on both defective and defect-free test images with different background textures, intensities, and different defect scales patterns are designed and the experimental results are shown in Fig. 5.

As illustrated in Fig. 5(u)–(x), for defect-free image no background texture edges are detected. In Fig. 5(d)–(h), 5(l), 5(p), and 5(t), all defects in test images are detected and located successfully with complete and accurate defect boundary edges. A few discontinuous and unclosed background texture edges as well as some noise are also detected which would be eliminated with morphology operations. Defects segmentation masks are generated from Fig. 5(b), 5(f), 5(j), 5(n), and 5(r) are shown in Fig. 5(c), 5(g), 5(k), 5(o), and 5(s). Fig. 5(d), 5(h), 5(l), 5(p), 5(t), and 5(x) show the final defect detection and segmentation results in which the defect boundary edges are highlighted.

Comparison results between conventional edge detection methods and the proposed method are shown in Fig. 6. Fig. 6(a) is the test image, and Fig. 6(b)–(h) show detection results using Sobel, LoG, Canny, Level set, Watershed, Scale space Blob, and SIFT features methods, respectively. These results illustrate that the conventional edge detection methods can only detect background texture edges partially and cannot discriminate defect edges and background textures. Image segmentation methods like Level set, Watershed and Scale space Blob detection methods cannot locate and segment the tire defect regions [Fig. 6(e)–(g)]. The extracted SIFT features are less effective for defect classification because the SIFT keypoint detector fails at finding sufficient features for classification in defect regions [Fig. 6(h)]. Fig. 6(i) shows detection result using the proposed scheme which illustrates that a complete and accurate defect segmentation mask is generated.

TABLE I
FALSE ALARM, NONDETECTION, AND SEGMENTATION ACCURACY OF THE PROPOSED SCHEME

Methods	Non-detection	False Alarm	Detection success rate	Number of samples
[38][a]	2.4%	2.8%	94.8%	200
[39][b, c]	4.2%	4.6%	91.2%	200
[25][d]	3.2%	7.3%	89.5%	200
Our method	1.3%	1.8%	96.9%	200

[a] Wavelet based method, [b] Morphological operation based method, [c] Gabor wavelet based method, [d] Dictionary representation based method.

The performance of the proposed scheme is determined by the nondetection rate, detection success rate and false alarm rate. We also give the overall normalized *EM* value which evaluates the localization accuracy and shape accuracy of detected defect edges. Based on all of the experiments carried out using our test data set, the detection success rate reached 96.9%, the normalized *EM* value reached as high as 0.915 on average and the false alarm rate is within 1.8% and the nondetected rate is within 1.3% as shown in Table I. Experimental results on tire radiographic image dataset using conventional morphological operation, wavelet, Gabor wavelet, and dictionary representation are given for comparison in Table I.

V. CONCLUSION

This paper studied the problem of tire defect detection based on wavelet multiscale analysis in radiography images. The characteristics of pneumatic tire radiography images are analyzed. Due to the multitextural characteristic of tire radiography images, we focus on the analysis of defect edges in high frequency multitextural background by using wavelet multiscale edge detection.

We presented a framework for selecting parameters of wavelet local modular maximum edge detection which was used for tire defect edge location. The scheme was efficient by using optimal parameters for online detection applications by virtue of its high overall detection rate, low false alarm rate, and location accuracy. The method is also not overly sensitive to the parameters for light-duty radial tires due to the tire industrial standard. Experiments were designed to validate the efficiency of the method, and a comparison with other existing methods is also provided. Further research can be conducted to apply the proposed method to solve a family of nondestructive test problems such as fabric defect detection, weld defect detection, and casting defect detection.

REFERENCES

[1] Y. Zhang, T. Li, and Q. L. Li, "Defect detection for tire laser shearography image using curvelet transform based edge detector," *Opt Laser Technol*, vol. 47, pp. 64–71, 2013.
[2] Y. Sun, P. Bai, H. Y. Sun, and P. Zhou, "Real-time automatic detection of weld defects in steel pipe," *NDT&E Int*, vol. 38, pp. 522–528, 2005.
[3] X. Li, S. K. Tso, X. Guan, and Q. Huang, "Improving automatic detection of defects in castings by applying wavelet technique," *IEEE Trans. Ind Electron.*, vol. 53, no. 6, pp. 1927–1934, Dec. 2006.

[4] H. Feng, Z. G. Jiang, F. Y. Xie, P. Yang, J. Shi, and L. Chen, "Automatic fastener classification and defect detection in vision-based railway inspection systems," *IEEE Trans. Instrum. Meas.*, vol. 63, no. 4, pp. 877–888, Apr. 2014.

[5] A. Kumar and G. K. H. Pang, "Defect detection in textured materials using Gabor filters," *IEEE Trans. Ind. Appl.*, vol. 38, no. 2, pp. 425–440, Mar./Apr. 2002.

[6] J. H. Oh, W. S. Kim, C. H. Han, and M. H. Park, "Defect detection of TFT-LCD image using adapted contrast sensitivity function and wavelet transform," *IEICE Trans. Electron*, vol. E90-C, pp. 2131–2135, 2007.

[7] L. Xu and Q. Huang, "Modeling the interactions among neighboring nanostructures for local feature characterization and defect detection," *IEEE Trans. Autom. Sci. Eng.*, vol. 9, no. 4, pp. 745–754, Oct. 2012.

[8] L. Xu and Q. Huang, "EM estimation of nanostructure interactions with incomplete feature measurement and its tailored space filling designs," *IEEE Trans. Autom. Sci. Eng.*, vol. 10, no. 3, pp. 579–587, Jul. 2013.

[9] M. Win, A. R. Bushroa, M. A. Hassan, N. M. Hilman, and A. Ide-Ektessabi, "A contrast adjustment thresholding method for surface defect detection based on mesoscopy," *IEEE Trans. Ind. Inf.*, vol. 11, no. 3, pp. 642–649, Jun. 2015.

[10] X. L. Bai, Y. M. Fang, W. S. Lin, L. P. Wang, and B. F. Ju, "Saliency-based defect detection in industrial images by using phase spectrum industrial informatics," *IEEE Trans. Ind. Inf.*, vol. 10, no. 4, pp. 2135–2145, Aug. 2014.

[11] Y. Zhang, T. Li, and Q. L. Li, "Detection of foreign bodies and bubble defects in tire X-ray images based on total variation and edge detection," *Chin. Phys. Lett.*, vol. 30, 2013, Art. ID 084205.

[12] B. Lucia, B. Giuseppe, P. Pisana, R. Elisa, S. Andrea, and V. Paolo, "Automatic defect detection in uniform and structured fabrics using Gabor filters and PCA," *J. Vis. Commun. Image R*, vol. 24, pp. 838–845, 2013.

[13] A. G. De, M. Meo, D. P. Almond, S. G. Pickering, and S. L. Angioni, "A new technique to detect defect size and depth in composite structures using digital shearography and unconstrained optimization," *NDT&E Int.*, vol. 45, pp. 91–96, 2012.

[14] G. Wang and T. W. Liao, "Automatic identification of different types of welding defects in radiographic images," *NDT&E Int..*, vol. 35, pp. 519–528, 2002.

[15] X. L. Li, S. K. Tso, X. P. Guan, and Q. Huang, "Improving automatic detection of defects in castings by applying wavelet technique," *IEEE Trans. Ind. Electron.*, vol. 53, no. 6, pp. 1927–1934, Dec. 2006.

[16] V. Lashkia, "Defect detection in X-ray images using fuzzy reasoning," *Image Vis. Comput.*, vol. 19, pp. 261–269, 2001.

[17] Y. T. N. Henry, G. K. H. Pang, and N. H. C. Yung, "Automatic fabric defect detection—A review," *Image Vis. Comput.*, vol. 29, pp. 442–458, 2011.

[18] Y. J. Lee and J. J. Lee, "Accurate automatic defect detection method using quadtree decomposition on SEM images," *IEEE Trans. Semicond. Manuf.*, vol. 27, no. 2, pp. 223–231, May 2014.

[19] Y. Y. Hung and R. M. Grant, "Shearography: A new optical method for nondestructive evaluation of tires," *Rubber Chemistry Technol.*, vol. 54, no. 5, pp. 1042–1050, 1981.

[20] X. Xiong, W. He, and H. Wang, "Digital image correlation method (DICM) application in speckle phase-shift of shear spechkle defect detection," in *Proc. Int. Symp. Intell. Signal Process. Commun. Syst.*, 2010, pp. 380–383.

[21] C. H. Chien, Y. D. Wu, Y. C. Chen, C. C. Hsieh, T. Chen, and Y. T. Chiou, "Quantitative detection of internal defects in automotive tires by an interferographic technique," *Res. Nondestructive Evaluation*, vol. 18, pp. 163–177, 2007.

[22] M. K. Ng, H. Y. T. Ngan, X. Yuan, and W. Zhang, "Patterned fabric inspection and visualization by the method of image decomposition," *IEEE Trans. Autom. Sci. Eng.*, vol. 11, no. 3, pp. 943–947, Jul. 2014.

[23] F. Y. Li, "The study of an improved fuzzy edge detection algorithm in the radial tire quality detection," *Adv. Mater. Res.*, vol. 317–319, pp. 968–971, 2011.

[24] A. Gayer and A. Saya, "The use of X-radiography and computer software for detecting defects during the manufacture of steel-belt tyres," *NDT Int.*, vol. 21, pp. 333–336, 1988.

[25] Y. Xiang, C. Zhang, and Q. Guo, "A dictionary-based method for tire defect detection," in *Proc. IEEE Int. Conf. Inf. Autom.*, 2014, pp. 519–523.

[26] D. Tsai and C. Chiang, "Automatic band selection for wavelet reconstruction in the application of defect detection," *Image Vis. Comput.*, vol. 21, no. 5, pp. 413–431, 2003.

[27] Y. Zhu, W. Y. Liu, F. C. Liu, and J. J. Wang, "Inspection of air bubble defect in tires by digital holography," *Opt. Prec. Eng.*, vol. 17, pp. 1099–1104, 2009.

[28] H. X. Liu, W. Zhou, Q. W. Kuang, L. Cao, and B. Gao, "Defect detection of IC wafer based on spectral subtraction," *IEEE Trans. Semicond.*, vol. 23, pp. 141–147, 2010.

[29] H. Y. T. Ngan and G. K. H. Pang, "Regularity analysis for patterned texture inspection," *IEEE Trans. Autom.. Sci. Eng.*, vol. 6, no. 1, pp. 131–144, Jan. 2009.

[30] D. Tsai and T. Huang, "Automated surface inspection for statistical textures," *Image Vis. Comput.*, vol. 21, pp. 307–323, 2003.

[31] Y. Han and P. Shi, "An adaptive level-selecting wavelet transform for texture defect detection," *Image Vis. Comput.*, vol. 25, pp. 1239–1248, 2007.

[32] K. L. Mak and P. Peng, "An automated inspection system for textile fabrics based on Gabor filters," *Robot Comput.. Integr. Manuf.*, vol. 24, no. 3, pp. 359–369, Jun. 2008.

[33] U. Farooq, T. King, P. H. Gaskell, and N. Kapur, "Machine vision using image data feedback for fault detection in complex deformable webs," *Trans. Inst. Meas. Contr.*, vol. 26, no. 2, pp. 119–137, 2004.

[34] C. J. Kuo and T. Su, "Gray relational analysis for recognizing fabric defects," *Textile Res. J.*, vol. 73, no. 5, pp. 461–465, 2003.

[35] H. Y. T. Ngan, G. K. H. Pang, and N. H. C. Yung, "Performance evaluation for motif-based patterned texture defect detection," *IEEE Trans. Autom. Sci. Eng.*, vol. 7, no. 1, pp. 58–72, Jan. 2010.

[36] S. Ghorai, A. Mukherjee, M. Gangadaran, and P. K. Dutta, "Automatic defect detection on hot-rolled flat steel products," *IEEE Trans. Instrum. Meas.*, vol. 62, no. 3, pp. 612–621, Mar. 2013.

[37] W. C. Li and D. M. Tsai, "Wavelet-based defect detection in solar wafer images with inhomogeneous texture," *Pattern Recogn.*, vol. 45, pp. 742–756, 2012.

[38] H. Y. T. Ngan, G. K. H. Pang, S. P. Yung, and M. K. Ng, "Wavelet based methods on patterned fabric defect detection," *Pattern Recogn.*, vol. 38, pp. 559–576, 2005.

[39] K. L. Mak, P. Peng, and K. F. C. Yiu, "Fabric defect detection using morphological filters," *Image Vis. Comput.*, vol. 27, no. 10, pp. 1585–1592, 2009.

[40] S. Mallat and S. Zhong, "Characterization of signals from multiscale edges," *IEEE Trans. Pattern Anal.*, vol. 14, no. 7, pp. 710–732, Jul. 1992.

[41] N. Merlet and J. Zerubia, "New prospects in line detection by dynamic programming," *IEEE Trans. Pattern Anal.*, vol. 18, no. 4, pp. 426–431, Apr. 1996.

[42] J. Hsieh, M. Ko, H. M. Liao, and K. Fan, "A new wavelet based edge detector via constrained optimization," *Image Vis. Comput.*, vol. 15, pp. 511–527, 1997.

[43] T. Aydin, Y. Yemez, E. Anarim, and B. Sankur, "Multidirectional and multiscale edge detection via M-band wavelet transform," *IEEE Trans. Image Process.*, vol. 5, no. 9, pp. 1370–1377, Sep. 1996.

[44] D. R. Waghule and R. S. Ochawar, "Overview on edge detection methods," in *Proc. IEEE Int. Conf. Electron. Syst., Signal Process. Computing Technol.*, 2014, pp. 151–155.

[45] C. L. Tu, W. L. Hwang, and J. Ho, "Analysis of singularities from modulus maxima of complex wavelets," *IEEE Trans Inf. Theory*, vol. 51, no. 3, pp. 1049–1062, Jul. 2005.

[46] M. Barakat, F. Druaux, D. Lefebvre, M. Khalil, and M. Mustapha, "Self adaptive growing neural network classifier for faults detection and diagnosis," *Neurocumputing*, vol. 74, no. 18, pp. 3865–3876, 2011.

[47] C. Ducottet, T. Fournel, and C. Barat, "Scale-adaptive detection and local characterization of edges based on wavelet transform," *Signal Process.*, vol. 84, no. 11, pp. 2115–2137, 2004.

[48] W. K. Pratt, *Digital Image Processing*. New York, NY, USA: Wiley, 1991.

[49] Y. Yue, M. M. Croitoru, A. Bidani, J. B. Zwischenberger, and J. W. Clark, "Nonlinear multiscale wavelet diffusion for speckle suppression and edge enhancement in ultrasound images," *IEEE Trans. Med. Imaging*, vol. 25, no. 3, pp. 297–311, Mar. 2006.

Yan Zhang received the B.S. degree in computer science and technology from Northwestern Polytechnical University, Xi'an, China, in 2004, and the M.S. and Ph.D. degrees in automatic control from Qingdao University of Science and Technology, Qingdao, China, in 2009 and 2014, respectively.

He is an Assistant Professor of electrical and computer engineering with Qingdao University of Science and Technology, Qingdao, China. He is currently a Visiting Scholar with the Research Group on Electrical Engineering and Automatic Control (GREAH), Faculty of Sciences, Normandy University, Le Havre, France. His research interests include digital image processing, pattern recognition and fault detection.

Dimitri Lefebvre graduated from the Ecole Centrale of Lille (France) in 1992. He received the Ph.D. degree in automatic control and computer science from the University of Sciences and Technologies, Lille, France, in 1994, and the HAB degree from University of Franche Comté, Belfort, France, in 2000.

Since 2001, he has been a Professor at Institute of Technology and Faculty of Sciences, Normandy University, Le Havre, France. He is with the Research Group on Electrical Engineering and Automatic Control (GREAH) and, from 2007 to 2012, he was the head of the group. His current research interests include learning processes, adaptive control, fault detection and diagnosis and Petri nets.

Qingling Li received the B.S. and M.S. degrees from Shandong College of Chemical Industry, Qingdao, China, in 1982 and 1989, respectively, and the Ph.D. degree from Huazhong University of Science and Technology, Wuhan, China, in 2004, all in mechanical engineering.

He is a Professor of mechanical engineering with Qingdao University of Science and Technology, Qingdao, China, and the Vice President of Qingdao University of Science and Technology. He was a Research Fellow with the Technical University of Munich, Munich, Germany, and University of Paderborn, Paderborn, Germany, during 1994 and 2000. His research interests include chemical process machinery and fault detection.